JOURNAL OF GEOPHYSICAL RESEARCH, VOL. 100, NO. C5, PAGES 8621–8637, MAY 15, 1995

Eddy- and wind-forced shelf circulation

Lie-Yauw Oey

Program in Atmospheric and Oceanic Sciences, Princeton University, Princeton, New Jersey

Abstract. Cochrane and Kelly (1986) proposed a cyclonic gyre as the large-scale mean circulation on the Louisiana-Texas (LATEX) shelf, produced by a convergence of coastal currents in the west and a divergence in the east. While currents near the coast are presumably wind and buoyancy driven, the origin of the eastward flow on the outer shelf and shelf break, which forms the seaward limb of the gyre, as well as the nearshore convergence and divergence, are not well understood. A numerical model is used to show that the western convergence and shelf break current are driven by collision and stalling of westward propagating Loop Current eddies in the northwest Gulf of Mexico and the divergence in the east is caused by shoreward intrusion in the Mississippi Canyon. The western convergence and shelf break current are modulated by the wind curl, strongest in summer and weakest in winter. On the shelf, westward transport is comparable to that observed (~0.15 Sv, 1 Sv = 10^6 m^3 s^{-1}) only when the westward wind stress is significant (>0.3 dyn cm^{-2}). A peak transport of 0.21 to 0.25 Sv occurs in autumn, of which 0.1 Sv is due to wind, 0.07 Sv is due to river buoyancy, and 0.04 to 0.08 Sv is due to eddies. Without the mean westward wind, buoyant waters from the Mississippi do not spread onto the LATEX shelf.

1. Introduction

The northern Gulf of Mexico shelf (Fig. 1), including the Louisiana-Texas (LATEX) shelf that we focus on in this study, is one of the nation's most fertile waters for fisheries and is also an area of extensive offshore oil and gas activity. As such, a study of the area's currents, temperature, and salinity is of interest.

The circulation and mixing in the LATEX shelf are influenced by a number of processes, including (1) buoyancy from rivers, (2) wind, and (3) forcing related to the Loop Current (LC) and Loop Current Eddies (LCEs). Owing to its high discharge of the order of 10^4 m^3 s^{-1} and weak tides, the Mississippi River discharges seaward above a sharp density interface [*Wright and Coleman*, 1971]. The effect of this freshening, plus contributions from other streams, the Atchafalaya River in particular, can be seen as a less saline coastal band along the LATEX coastline and covering nearly half the width of the shelf [*Cochrane and Kelly*, 1986] (hereinafter referred to as CK). There is a strong interaction between buoyancy-driven and wind-induced shelf currents. On the basis of hydrographic measurements, CK shows how wind variability can change the shelf salinity patterns in different seasons. Except during the summer, the most prominent shelf circulation is inferred to be cyclonic, westward nearshore, and eastward on the outer shelf and shelf break. This circulation is set up as a result of coastal current convergence at the southwestern limb of the gyre off Texas/Mexico and divergence at the eastern limb just west of the Mississippi Delta. The nearshore flow is induced by west/southward wind which prevails most of the year except in July–August. The cause for the eastward flow on the outer shelf is more uncertain; in fact, its existence may be questioned by those critical of inferences obtained from dynamic height calculations. In support of the inferred gyre, CK quoted a number of direct current meter measurements on the outer shelf and shelf break which showed eastward flow.

The seaward limb of the cyclonic gyre lies over the shelf break and outer shelf, where satellite imagery shows a fairly strong cross-shelf thermal contrast (F. M. Vukovich, private communication, 1995). The circulation seaward of the shelf break in the northwestern Gulf is often dominated by cyclonic and anticyclonic eddies (see, e.g., *Brooks* [1984]), reminiscent of, perhaps, the LCEs and offsprings. One expects that eddies exist also along the entire LATEX shelf break from farther east, the most obvious of which are westward propagating LCEs. Therefore it seems reasonable to hypothesize that the outer shelf and shelf break flows are in some way influenced by basin-scale forcing of the LC and LCES.

Besides eddies, *Sturges* [1993] has argued that wind stress curl drives a seasonal boundary current in the western Gulf, most evident in the ship-drift data between 23° and 26°N during summer. The LATEX shelf break current can simply be a manifestation of the boundary current by its continuity around the northwest corner and eastward.

The main objective of the present study is to use a numerical model to explain how wind, eddies, and buoyancy generate the mean cyclonic gyre on the LATEX shelf. To accomplish this, I analyze the following two groups of experiments: one driven by LCEs, steady wind, and river, and the other by variable wind, with and without river, and excluding LCEs. The former isolates LCE variability, while the latter is used to study the seasonal response.

The next section briefly describes the model. Section 3 discusses how LCEs can drive a shelf break current, and section 4 gives a preliminary analysis of wind, eddy, and buoyancy effects. Section 5 examines the effect of seasonal wind stress curl and discusses in detail the roles of eddies, wind, and river on shelf and shelf break transports. The paper concludes with section 6.

Paper number 95JC00785.
0148-0227/95/95JC-00785$05.00

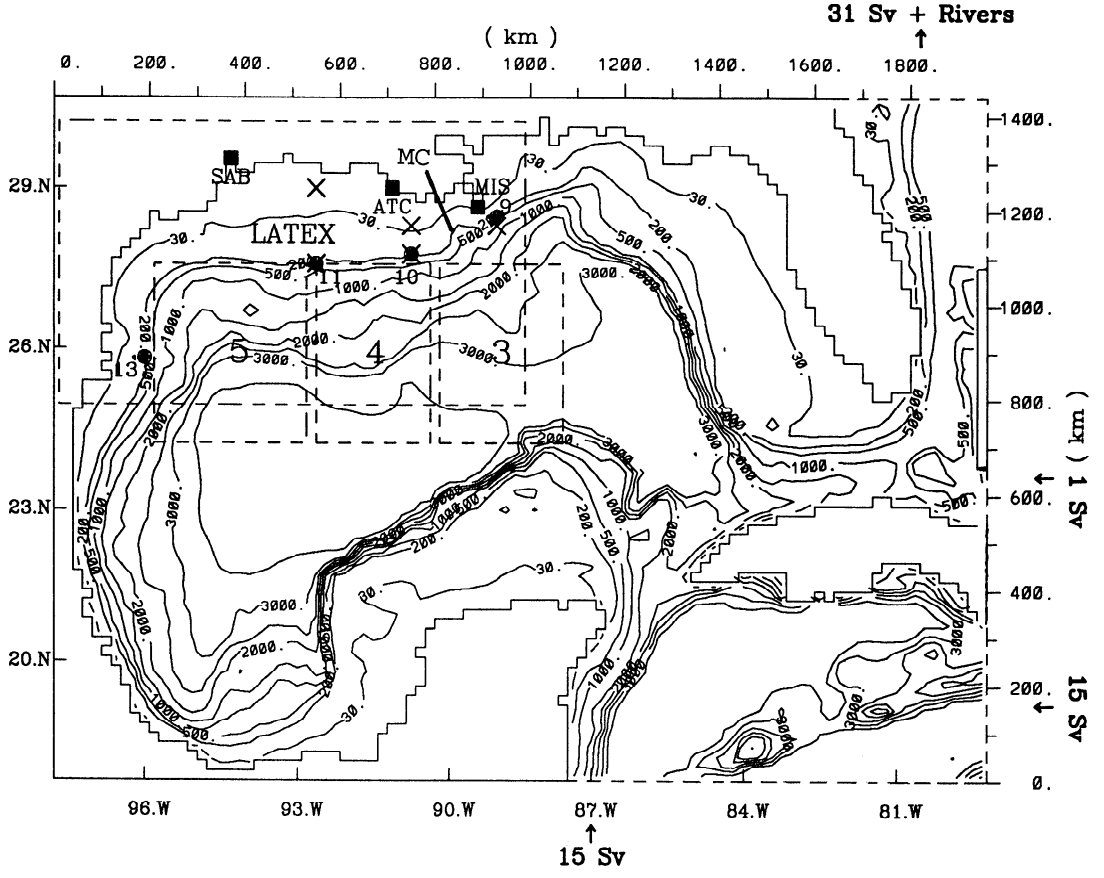

Figure 1. The Gulf of Mexico model domain and isobaths in meters. Abbreviations are MC, Mississippi Canyon (squares indicate river discharge points); MIS, Mississippi; ATC, Atchafalaya; and SAB, Sabine plus others. Regions of the Louisiana-Texas (LATEX) shelf/slope and where averaged vorticities are calculated are enclosed by dashed rectangles. Solid circles are stations where currents are studied in detail in text, and crosses are where momentum balances are computed in Table 1.

2. The Model

I use the *Oey and Chen* [1992a, b] version of the *Blumberg and Mellor* [1983] three-dimensional (3-D), primitive equation ocean model. The scheme is finite difference, centered-space, and leapfrog in time and computes three velocity components (u, v, and w), temperature T, salinity S (hence density ρ), and surface elevation η. Figure 1 shows the model domain, as well as locations where the (constant) inflow and outflow transports are specified at the open boundaries in the Caribbean and the South Atlantic Bight and where river discharges are specified at three sites along the LATEX coast. The grid sizes are 20 km, both in the x (east/west) and y (north/south) directions, and there are 20 equally spaced σ cells in the vertical. *Oey* [1994] has conducted fairly extensive sensitivity experiments on the model solutions to horizontal mixing and other model parameters and showed that the modeled LC sheds eddies at irregular periods of 6–20 months, with an average of about 8–13 months depending on the values of the horizontal mixing. The modeled LCES, though somewhat weaker than observed LCES in terms of the peak surface currents, have otherwise approximately the right sizes (~300 km), westward propagating speeds (~4 km d^{-1}), and tracks. Other Gulf-scale responses in terms of topographic Rossby and trapped Kelvin wave propagation forced by LC and LCE variability also appear to have their counterparts in observations.

In the first (sections 3 and 4) of the two groups of experiments the model is forced by climatological surface fluxes averaged over February, March, and April (wind stress $\approx$ 0.3 dyn cm^{-2} westward over LATEX), and fluctuations are therefore caused by LC and LCEs. The results are taken from two of the seven 10-year experiments presented by *Oey* [1994] (experiments C2 and C4), with horizontal mixing coefficient of the order of 10–50 m^2 s^{-1} over the shelf and from other shorter-duration experiments specific to this paper. In the second group (section 5) I focus on the effects of variable wind stress curl by forcing the model with the European Centre for Medium-Range Weather Forecasts (ECMWF) wind for 1985–1990 (courtesy of J. Herring) and by setting the Yucatan inflow to zero (i.e., turning off LC and LCEs). In this paper, "shelf and slope" will refer to those of LATEX only.

3. Shelf Break Current due to Eddies

3.1. The Forcing

To omit initial transients, the first 3 years of the 10-year calculation were skipped and the last 7 years were then averaged. The results (Figure 2) show a cyclonic gyre over

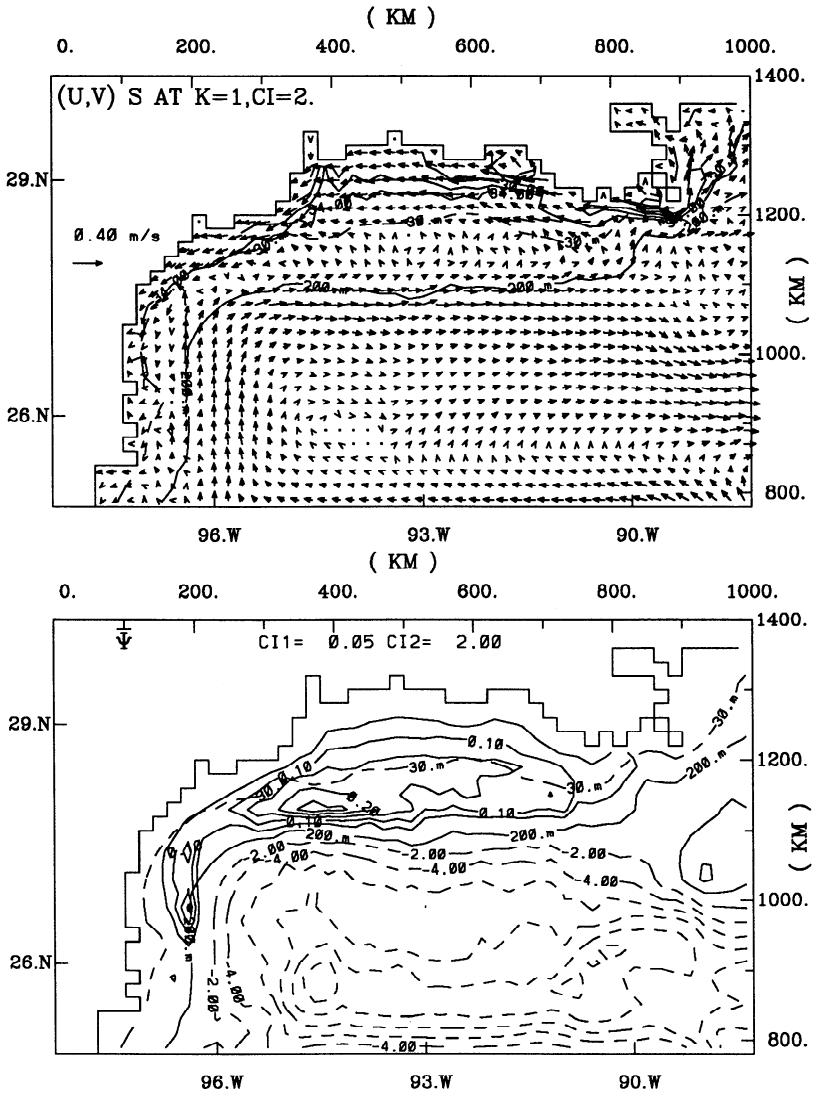

Figure 2. Seven-year-averaged surface (top) currents and (bottom) stream function (in sverdrups) over the LATEX region (years 3 through 10).

the LATEX region. The currents are westward from coast to midshelf (~30 m), and the transport magnitude of ~0.15 Sv (1 Sv = 10^6 m^3 s^{-1}) agrees with the estimate from LATEX current measurements (R. O. Reid, private communication, 1994). Over the shelf break and slope the current is eastward, ~0.1 m s^{-1}, and the maximum transport is ~6 Sv. I now describe two ways in which eddies can force transient eastward flows along the shelf break, the totality of which constitutes the seaward limb of the cyclonic gyre over the shelf.

3.1.1. Forcing by LC expansion and LCE passage. Figure 3 shows examples of 5-day averaged currents at vertical distance axis $z = -150$ m during a LC expansion and LCE shedding cycle. LATEX currents are weak prior to the shedding (Figure 3a). An eastward current trapped along the shelf break is produced as the LC expands (Figure 3b); the forcing is southeast of the Mississippi River Delta, and the response is in the form of free and forced trapped waves [*Oey*, 1994]. The current is anticyclonic, the same sense as the forcing. Once shed, the LCE continues to force the shelf break current (SC) as it propagates westward (Figure 3c). The eastward current subsides as the LCE collides with the western slope (Figure 3d). The process lasts about 8 months. The average shedding period for this experiment is 14 months, and one can expect a significant eastward current to be generated by this process.

3.1.2. Forcing by LCE collision at the northwestern Gulf. Analyses of the LCE in Figure 3d as it approached the western slope revealed that its southwestward movement was caused by interaction with a cyclone to its south. In the absence of such interaction the majority of the model eddies migrated north, then east, around the northwest corner of the Gulf. *Shi and Nof* [1993] described such a migration using both the contour dynamics and isopycnic primitive equation models on an f plane (Figure 4). The wall (i.e., continental slope) splits the eddy into two with opposite signs. For an annulus not thicker than about the inner core radius (Figure 4) an anticyclone consisting primarily of fluid of the inner core migrates to the right (looking onshore) at a speed of ~4 km d^{-1}, and a cyclone consisting of the annulus fluid moves to the left. When the annulus is thicker than core radius, splitting still occurs except the cyclone is much

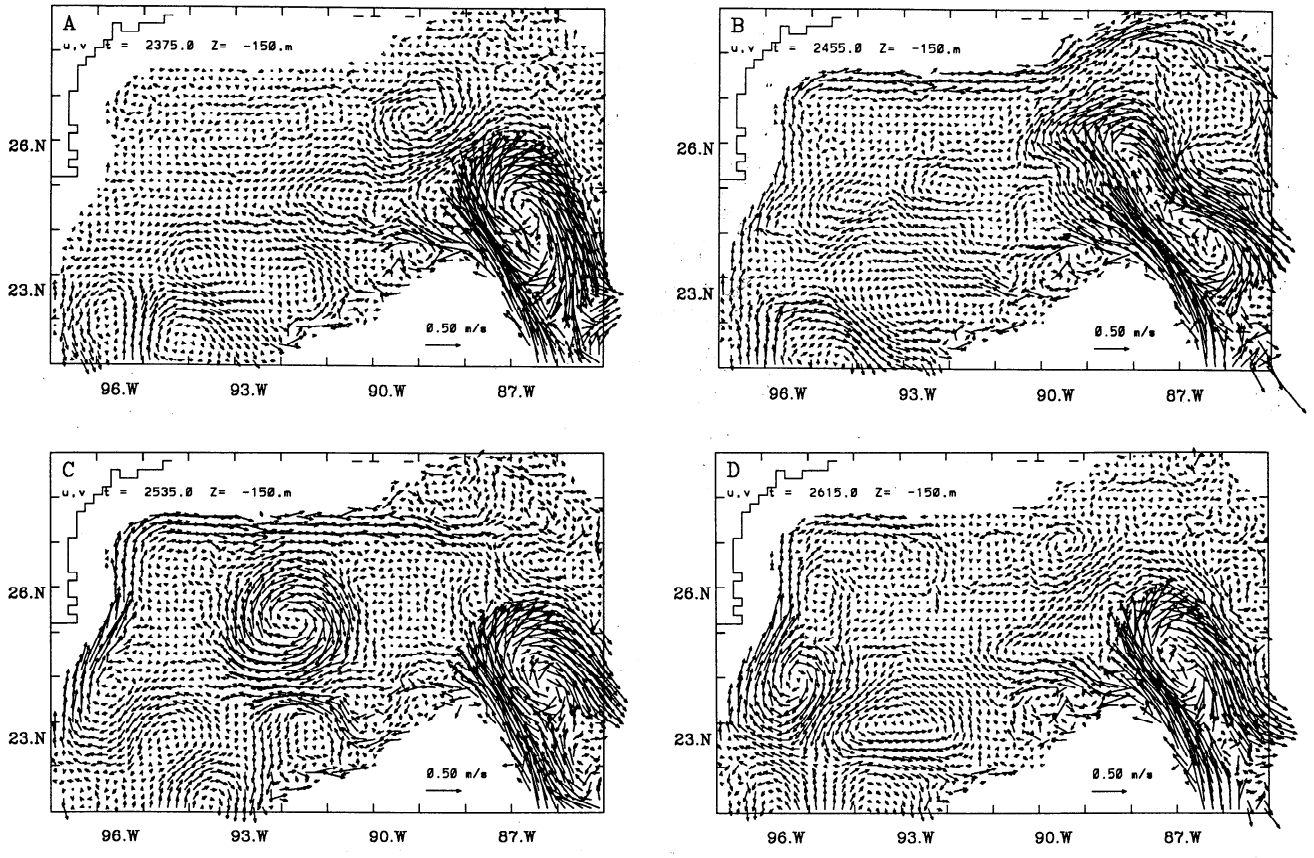

Figure 3. Modeled velocity vectors at vertical distance axis $z = -150$ m and time $t =$ (a) 2375, (b) 2455, (c) 2535, and (d) 2615 days.

smaller and the anticyclone becomes stationary. These behaviors are caused by wall image effects [*Shi and Nof*, 1993].

Figure 5 shows elevation contours, at 20-day intervals, of a LCE as it propagates westward and collides with the western slope. Each contour represents the approximate outline of the eddy at that instant, and to allow for eddy decay, different contour values are chosen for different times. After the collision at $t \approx 3470$ days the eddy migrates

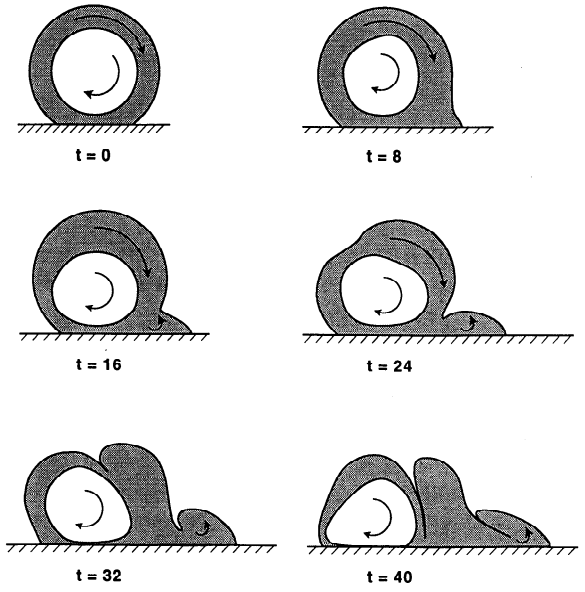

Figure 4. The evolution of an anticyclone colliding with a wall (adapted from *Shi and Nof* [1993]). The vorticity is anticyclonic in the inner core and cyclonic in the annulus (shaded).

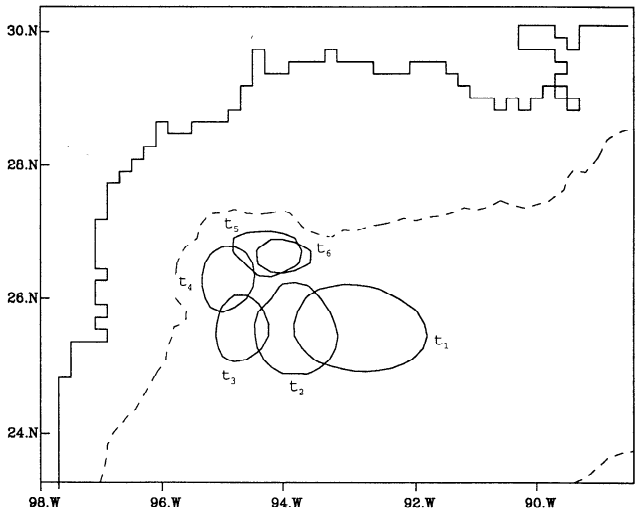

Figure 5. Elevation contours at 20-day intervals beginning from $t_1 = 3430$ days of a Loop Current Eddy (LCE) as it propagates westward and collides with the western slope. Contour values for t_1, t_2, and t_3 are 0.2 m, and they are 0.15, 0.1, and 0.05 m for t_4, t_5, and t_6, respectively. Dashed contour shows the 1000-m isobath.

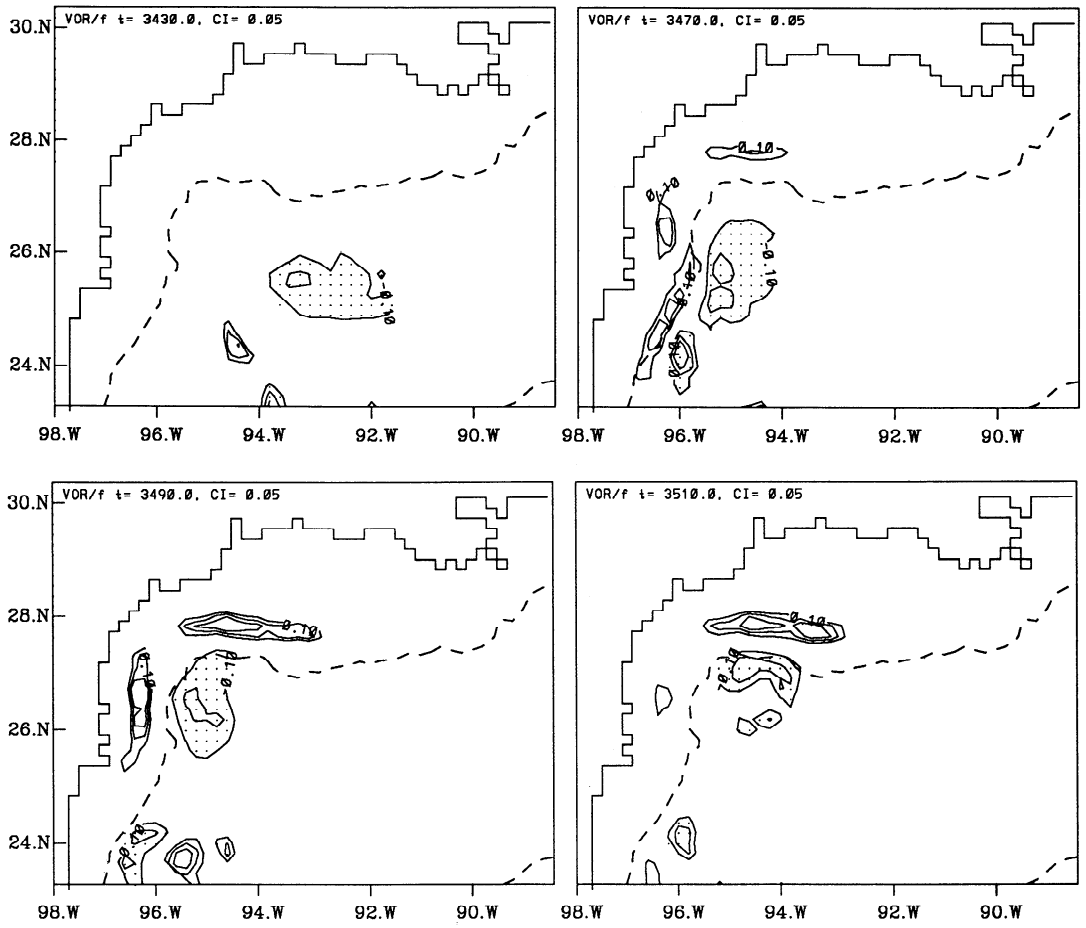

Figure 6. Contours of vorticity (nondimensionalized by Coriolis parameter) that illustrate image effects during eddy collision with the slope. Dashed contour shows the 1000 m isobath.

northward to the corner, then eastward. The migration is 170 to 200 km in 40 to 60 days or a speed of ~3.3 to 4.4 km d^{-1}. The behavior is similar to that described by *Shi and Nof* [1993]. The eddy stalls and decays rapidly after it turns eastward around the corner. The image effect can be illustrated by means of vorticity plots as shown in Figure 6. As the eddy collides with the western slope (t = 3470), image cyclones are produced to the west and north over the shelf. The cyclone/anticyclone pair moves northward to the corner (t = 3490), at which time the north shelf cyclone strengthens. At a later time (t = 3510), eastward migration continues as the north shelf cyclone persists while the west shelf cyclone weakens.

Figure 7 gives the corresponding near-surface currents, salinity, and temperature, as well as the elevation, superimposed on the depth-averaged velocities at time t_1 = 3430 and t_4 = 3490 days. A comparison of the currents indicates that the collision and stalling process (t_4) produces SCs quite distinct from those due to eddy passages (t_1), though in a time series it may be difficult to distinguish between them. As the eddy collides, a strong thermal front develops on the west shelf. Clearly, the local west shelf circulation, which was produced by wind and buoyancy prior to collision (t_1, as evidenced by close resemblance of the salinity and temperature contours), is now dominated by the eddy. The S = 35 psu contour, for example, is advected northward and against the inner shelf.

I conclude that LCE collision events can dominate shelf circulation in the corner region. Moreover, the northwestern Gulf is a "graveyard" for LCEs.

3.2. The Structure

I first demonstrate the robustness of the above relationship between eddy passages/collisions and SCs by showing time series. The vertical current structures are next shown via empirical orthogonal function (EOF) analysis.

Figure 8 (top and middle) shows the fluctuating parts of the along- and across-isobath components, respectively, of currents at shelf break stations 10, 11, and 13 (Figure 1). The means and standard deviations are given next to each curve. Figure 8 (bottom) shows relative vorticities averaged over regions 3, 4, and 5 (Figure 1). Fluctuations are caused by LC expansions/contractions (e.g., Figure 3b, which do not always result in eddy shedding) and/or LCE passages/collisions (Figures 3c and 3d). Positive peaks in along-isobath components correspond to negative vorticity peaks indicative of LC expansions and/or eddy passages, especially after year 5. The along-isobath fluctuations have peaks of ±0.15 m s^{-1}, and means are eastward at stations 10 and 11 and northward at station 13, with a maximum of 0.18 m s^{-1} at station 11. The across-isobath components are weaker, with fluctuations of about ±5 cm s^{-1}, and the peaks and troughs are apparently eddy-induced. Cross-spectrum analyses between the velocities and vorticities give a squared coherency

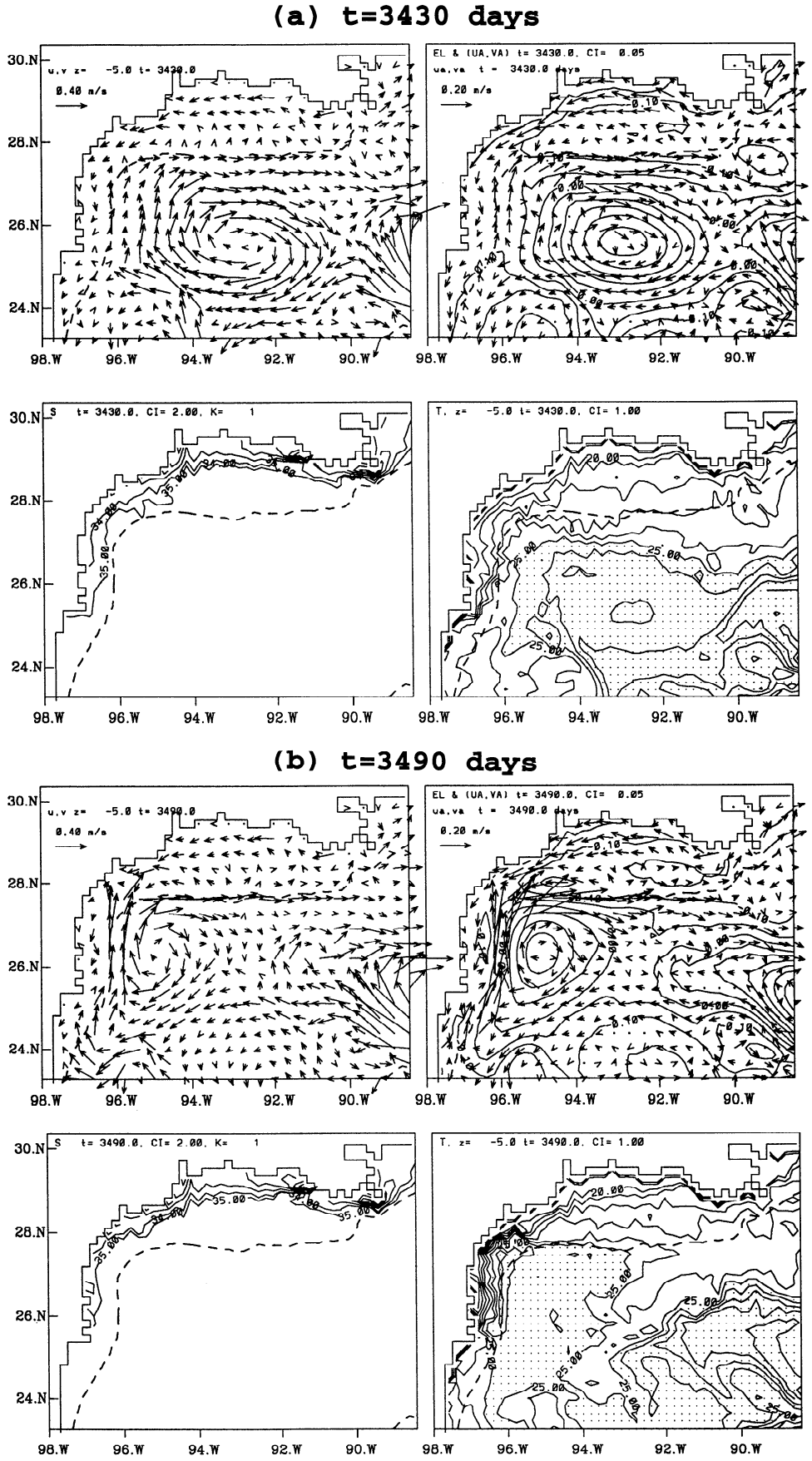

Figure 7. (clockwise from top left) Velocity vectors at $z = -5$ m, depth-averaged vectors with elevation superimposed, temperature T at $z = -5$ m (stippled where $T > 25$°C), and salinity for the near-surface sigma grid at (a) $t = 3430$ and (b) $t = 3490$ days.

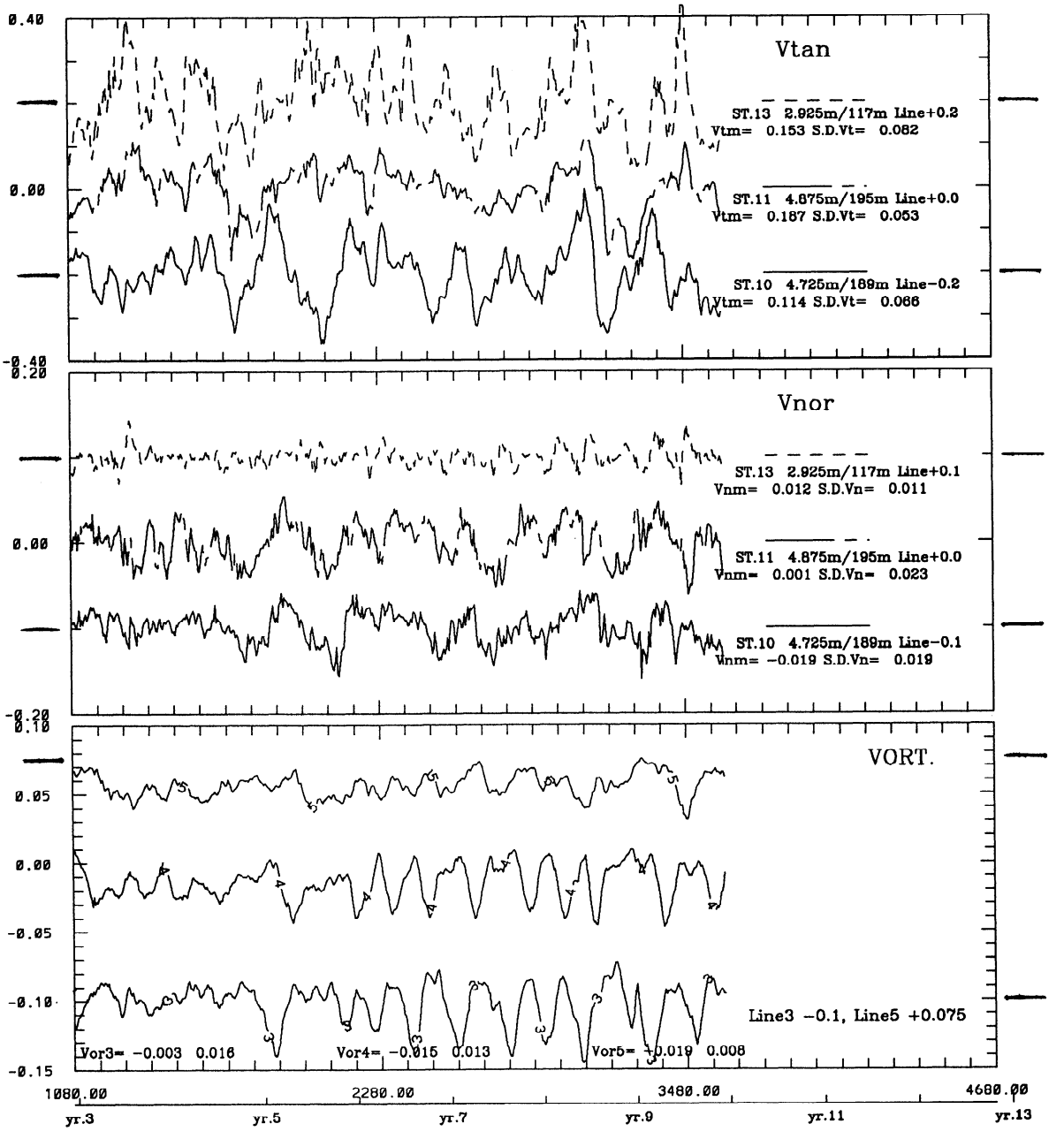

Figure 8. The fluctuation components of (top) along-isobath and (middle) across-isobath (positive offshore) currents at shelf break stations 10, 11, and 13 (see Figure 1). (bottom) Relative vorticities averaged over regions 3, 4, and 5 (see Figure 1). The top and bottom curves in each panel have been shifted (for clarity) by amount shown on the y axes. Information on right-hand side includes station number, depth of current/water depth, shift values, and mean and standard deviation of current.

of 0.4 near 50- to 100-day periods at the 95% significance level; values are smaller at station 11, especially for the across-isobath component. The means of the across-isobath component are offshore at station 13, onshore at station 10, and weak (offshore) at station 11. The net effect is therefore an influx onto the shelf in the eastern portion of LATEX and offshore flux in the southwest (compare Figure 2).

The vertical structures of the currents are shown in Figure 9. This gives stick plots at various depths and vertical EOFs of the along-isobath component at stations 9 and 10. Data collected by the Texas A&M University, Gulfcet 6 cruise [*Fargion and Davis*, 1994] indicates low-salinity values (34 psu) some 70 km south of the Mississippi Delta in waters of 500 m and more. This is consistent with the modeled current at station 9, which shows westward near-surface flow associated with the Mississippi River plume. There is also significant baroclinicity, especially when compared with currents at station 10 (and also with currents at other shelf break stations farther west). The first EOF mode at station 9 contains 78% of the total energy, with about 11% from the second and third modes. At station 10, on the other hand, the first mode contains ~95% of the energy, and higher modes are small.

To illustrate the dynamics, I tabulate (Table 1) values of

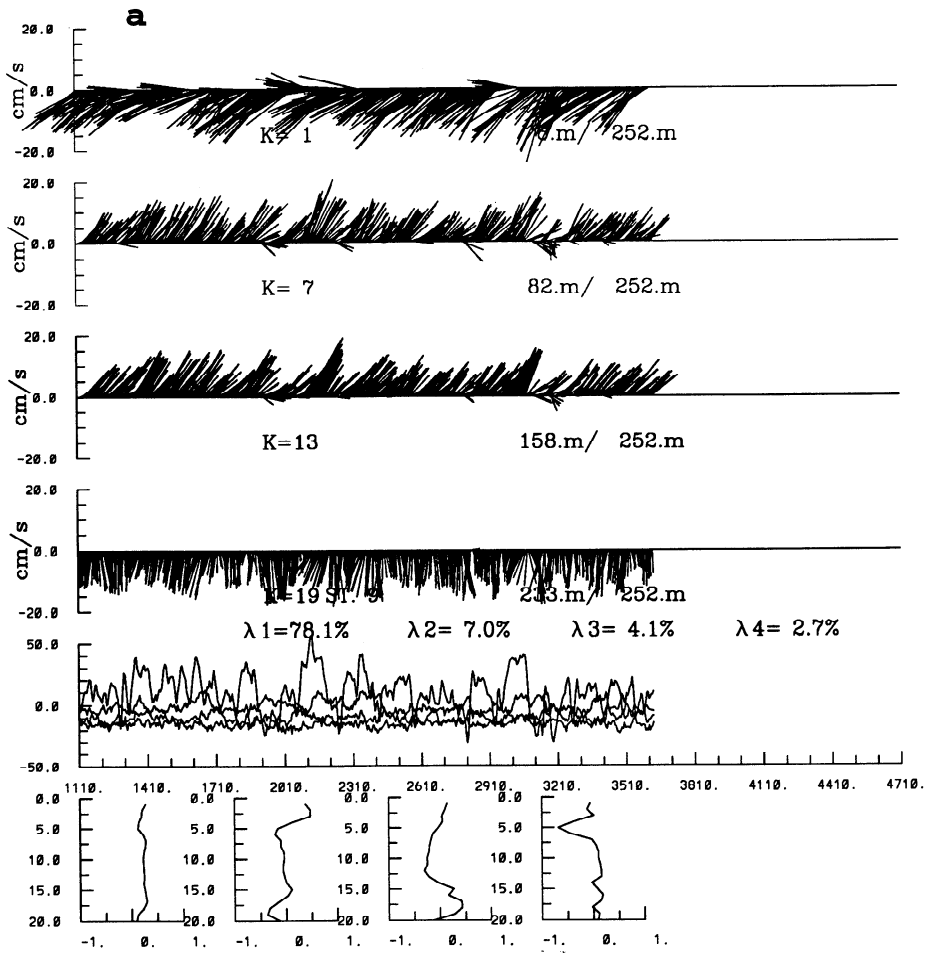

Figure 9. Stick plots (labeled cm/s) at various depths and the vertical empirical orthogonal functions of the along-isobath component at (a) station 9 and (b) station 10. Sticks point upward for positive along-isobath component defined as 50° and 90° from true north for stations 9 and 10, respectively. The across-isobath component is positive offshore. The λ_n is percent energy in mode "n."

terms in the cross-shore momentum balance near the surface, at stations 9, 10, and 11, and locations marked with a cross in Figure 1. For terms 3 and 5 I also give in brackets the corresponding depth-averaged values, −term 3 ≈ terms 4 + 5 for geostrophic balance. Nearshore at stations 10 and 11, sea levels slope upward toward shore (negative term 4), produced by cross-shore salinity contrasts. Except for the vertical shear and advection terms at the nearshore locations at stations 10 and 11, which are quite significant, these slopes are primarily balanced geostrophically by Coriolis force due to the westward currents. Over the outer shelf and shelf break at stations 10 and 11 the slopes change signs and become downward toward shore. These slopes are produced by warm waters of the LCEs to the south and are balanced geostrophically by eastward currents along the shelf break. At station 9, on the other hand, sea level slope remains upward toward shore at locations over the 225- and 500-m water depths, and geostrophic currents are westward, similar to the near-coast locations at stations 10 and 11. Thus the westward current at station 9 is caused by the Mississippi River plume, while eastward currents farther west are dominated by LCE-related processes. Taken together with the results of Figure 8, I conclude that the confluence of these currents produces a near-surface convergence on the outer shelf at ~90°W, i.e., between stations 9 and 10 in Figure 1. While I discussed only the effects of LCEs and river plume, it is reasonable to speculate that the shelf break topography of the Mississippi Canyon in this vicinity has a channeling effect on the flow, which can enhance on-shelf flux (see below).

4. Eddy Versus Wind/Buoyancy Effects

The last 1.4 years of the model run of Figure 2, from year 8.6 through 10, was repeated without the wind. The objective is to obtain a wind-alone solution (Figure 10) by subtracting this solution (eddy plus buoyancy) from that of Figure 2 (wind plus eddy plus buoyancy). The analysis is not without ambiguity, since near the coast the differenced field contains both the wind- and buoyancy-driven components, and there may also be an interaction between the wind and LCEs. Nonetheless, the results are informative and can be compared with those from a more precise analysis in later sections. A comparison of Figures 2 and 10a shows that the stream function is modified by eddy effects, both in the east in the vicinity of the Mississippi Canyon, where westward flow is increased when eddies are absent (Figure 10a), and also in the southwest, where net transport due to eddies is

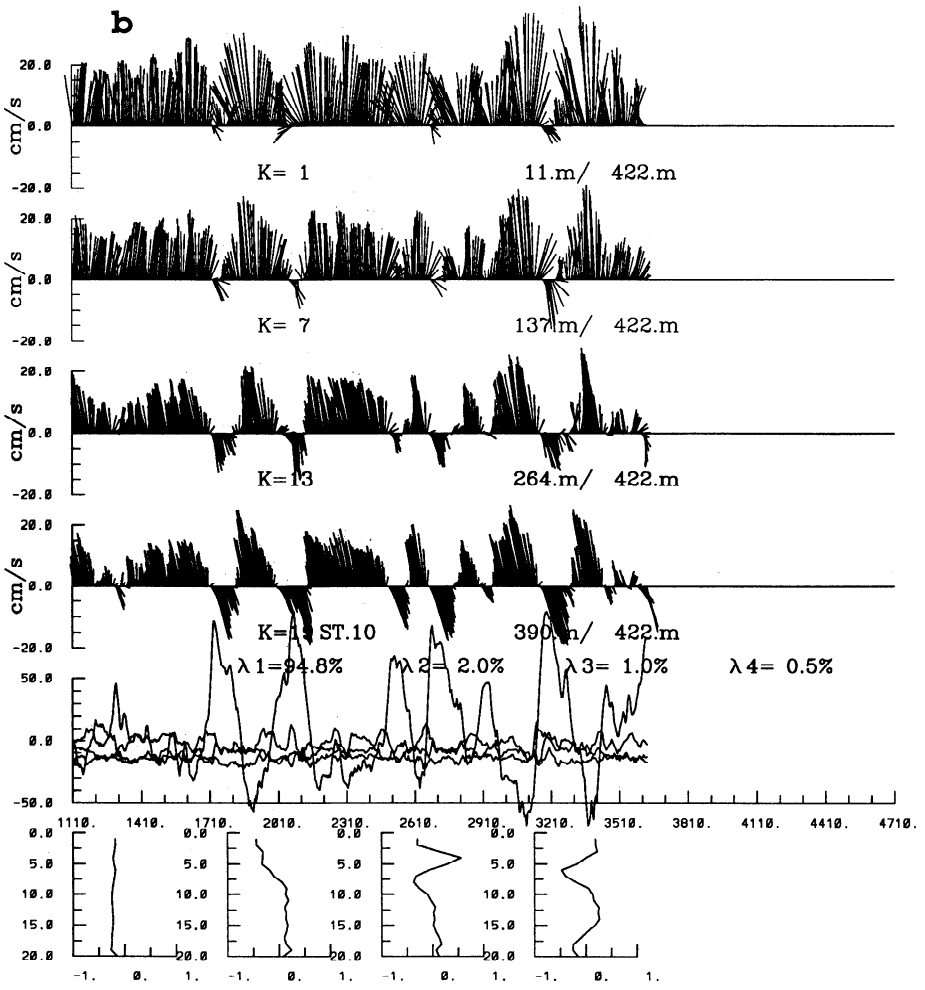

Figure 9. (continued)

northward over the outer shelf and shelf break. The streamlines in the southwest form a close loop (Figure 2) instead of being parabathic if wind and buoyancy were to act alone (Figure 10a). A comparison of the depth-averaged vectors and surface elevation contours (Figure 10b) shows also that the shelf current is predominantly barotropic and geostrophic. The characteristics are similar to *Csanady*'s [1978] arrested topographic wave solution, with the origin of the downshelf pressure distribution located near 92°W. In the absence of eddies, transport in the Mississippi Canyon is offshore as shown by the depth-averaged velocity vectors in Figure 10b (top), while those for the solution without wind show onshore flow (Figure 11). Thus LCEs generate eastward SCs, which in turn transport Gulf waters onshore near the canyon. This onshore flux serves as an important link which closes the eastern limb of the shelf's cyclonic gyre in the CK mean circulation scheme. However, the transport veers eastward to south of the Mississippi Delta and farther east. I conclude from this and from the stream functions in Figures 2 and 10a that westward shelf transport is primarily wind- and buoyancy induced and that wind alone is insufficient to generate a SC. These conclusions, while generally correct, are tentative and will be modified below by a more precise analysis which includes the seasonal variability of the wind.

The effect of wind and buoyancy interaction is illustrated in Figure 12, which shows the near-surface salinity contours at t = 3630 days (other times are similar) for the experiments with and without wind (Figure 12, top and bottom, respectively). In the absence of wind the Mississippi River plume veers eastward into the Mississippi-Alabama shelf, driven by the eddy-induced eastward current along the outer shelf and shelf break (see Figure 11). As a result, buoyant waters do not extend onto the Texas/Mexico shelf as in the case with wind forcing. Thus the prevailing mean westward wind is crucial in transporting waters of Mississippi River origin onto the LATEX shelf. We see also that we do not obtain a wind-alone solution by simply subtracting the top from the bottom of Figure 12.

5. Effects of Seasonal Wind

Sturges [1993] presented wind and ship-drift data which indicated a seasonally varying western boundary current (WBC) between 23° and 26°N. The strongest northward current in July lagged the maximum anticyclonic wind stress curl by ~1–2 months. Since LCE shedding did not display an annual signal, Sturges concluded that the current was driven by the wind curl. The focus was on the western Gulf, and it was not clear if the WBC continued around the northwest corner of the Gulf and eastward along the LATEX shelf break. Nonetheless, his study suggests that seasonal variability of the wind may be important.

Table 1. Cross-Shelf Momentum Balance at Stations 9, 10, and 11 and at Locations Marked With a Cross in Figure 1

	Cross-Shelf Momentum Terms, $\times 10^{-6}$ m/s^2						
Water Depth, m	1, $\partial v/\partial t$	2, $-\mathbf{u}\cdot\nabla v$	3, $-fu$	4, $-g\partial\eta/\partial y$	5, $-g[\int_z^\eta \partial\rho/\partial y\, dz]/\rho_0$	6 = 4 + 5, $-(\partial p/\partial y)/\rho_0$	7, $\partial(K\partial u/\partial z)/\partial z$
				Station 9			
225	...	...	7.2	−8.9	1.0	−7.9	...
			(2.1)		(6.6)		
500	...	...	1.7	−1.7	0.3	−1.4	...
			(1.3)		(−0.2)		
				Station 10			
22	...	1.0	8.2	−6.0	0.2	−5.8	−2.5
			(2.7)		(3.4)		
189	...	...	−7.0	7.3	0.1	7.4	...
			(−5.5)		(−2.7)		
422	...	...	−7.1	6.0	0.6	6.6	...
			(−2.0)		(−4.4)		
				Station 11			
5	...	1.0	15.7	−14.4	0.3	−14.1	−1.5
			(8.4)		(5.7)		
195	...	...	−8.6	8.6	0.2	8.8	...
			(−6.5)		(−2.0)		
570	...	...	−6.6	4.0	2.0	6.0	...
			(−6.7)		(2.7)		

Variables are defined as follows: **u**, velocity vector; t, time; f, Coriolis parameter; g, gravitational acceleration constant; η, surface elevation; y, north/south distance (positive northward); ρ, density; p, pressure; K, vertical eddy viscosity coefficient; and z, vertical distance axis (positive upward). Dots indicate values less than 10^{-7} m/s^2. Numbers in parentheses are the corresponding depth-averaged values.

We focus on the seasonal variability by analyzing the results of a 5-year (1985–1990) model run forced by 6-hourly wind stress obtained from the ECMWF and by zero Yucatan inflow (i.e., no LC and LCEs). The initial state was quiescent, with flat isopycnals obtained from horizontally averaging the *Levitus*' [1982] winter 3-D density field (i.e., that of the experiments in previous sections). The model was integrated from this state for 30 days to ensure that the velocities remain small (maximum of O (mm s^{-1})) and continued with the wind (case 1) and wind and river buoyancy (case 2) turned on.

5.1. Shelf Break Current

The model results show a seasonal current that is northward in the western Gulf, eastward along the LATEX shelf break, and southward (i.e., seaward) southeast of the Mississippi Delta (the EGulf, ~86°–89°W and 26°–28°N). An example for case 1 in July is given in Figure 13 (case 2 shows similar features). The current is most intense during the summer, forced in part by wind curl to the east. Figure 14 summarizes the seasonal response of the model WBC and SC to wind. Depths in the WGulf, LATEX, and EGulf regions range from 200 to 3500 m, 200 to 2000 m, and 3200 to 4000 m, respectively, so that points where depths are less than 200 m are excluded. Figure 14 shows that negative wind stress curls reach a maximum in May–July. This is followed by increases in the northward and eastward currents (and transports), in the WGulf and LATEX regions, respectively, with 1 to 2 months lag. From May through August the SC and EGulf currents increase in strength syncronous with the WBC, and continue to increase through October even as the WBC transport weakens. Thus the SC is only partly forced by the WBC in early summer and is sustained by forcing from farther east in the EGulf. The forcing is in the form of a decreased anticyclonic wind curl which becomes cyclonic from September through October over the EGulf (Figure 14). This induces localized upwelling (T at $z \approx -500$ m decreases by about 0.6°C from June through October), increased east-to-west thermal gradient (0.56°C per 20 km in September), and results in intensified southward flow in the EGulf, hence eastward current along the LATEX shelf break.

5.2. LATEX Shelf Transport

Westward transport increases when westward wind component strengthens and also when rivers are included (case 2). Examples of these responses are illustrated in Figure 15 with depth-averaged vectors for July and October, and Figure 16 shows time series which summarize how wind, buoyancy, and eddies contribute to the total shelf transport. Figure 15 shows that in July the shelf transport is confined off the Texas/Mexico shelf, where it is northward related apparently to wind from the southeast (Figure 16a) and is weak over the LATEX shelf. In October, westward flow is seen over the LATEX shelf and strengthens with inclusion of rivers (compare Figure 15, middle and bottom). Figure 16 shows that wind and transport are related. The maximum westward transport occurs in October when the westward wind stress is strongest. The shelf transport is weak in summer as wind is generally onshore and the largest transport is confined over the shelf break (Figure 15). River increases the transport (seen as downward shifting of the solid curves with respect to the dashed curves in Figure 16) by the additional 0.02 Sv discharge and also by increased flow which results when stratification effectively reduces friction. The former appears dominant in winter through summer, and the latter is seen in fall when westward wind is strong. The fall period is therefore when interaction between wind and river buoyancy is most significant. At the peak of this interaction in October, transport increases by ~50%

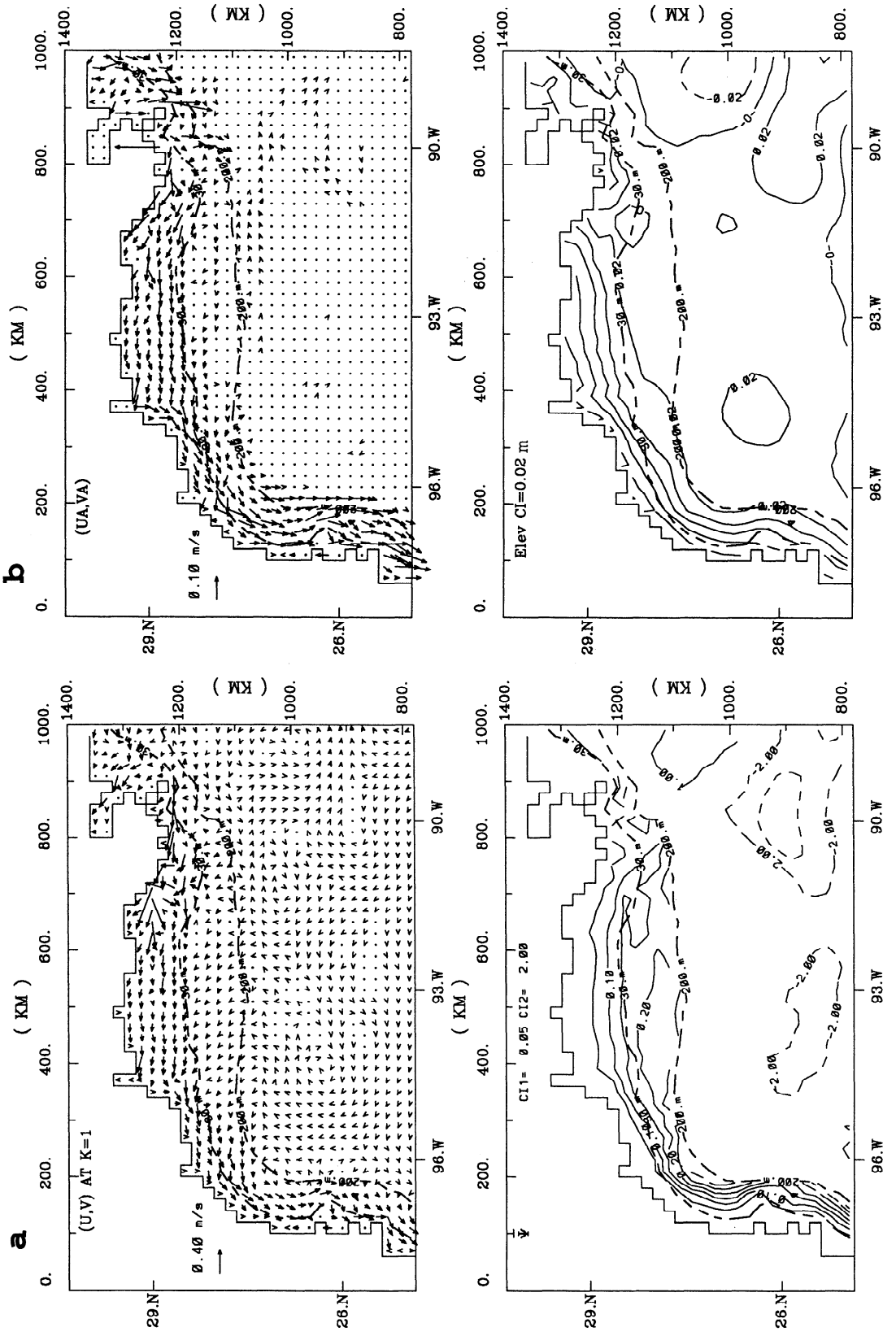

Figure 10. (a) The averaged differenced fields for (top) vectors at surface sigma grid and (bottom) stream function (in sverdrups) between a solution with (see Figure 3) and without wind. Averaging is for 480 days. (b) Same as Figure 10a, but for (top) depth-averaged vectors and (bottom) elevation.

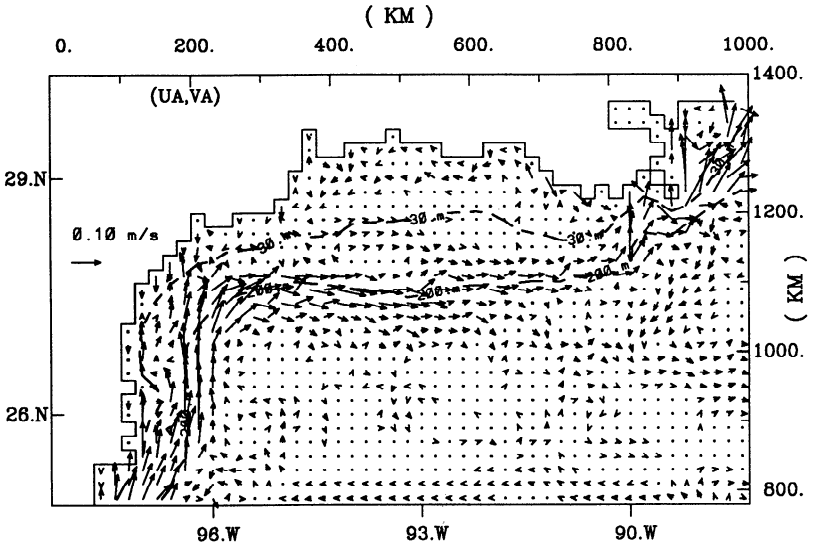

Figure 11. The 480-day mean depth-averaged vectors for the solution without wind.

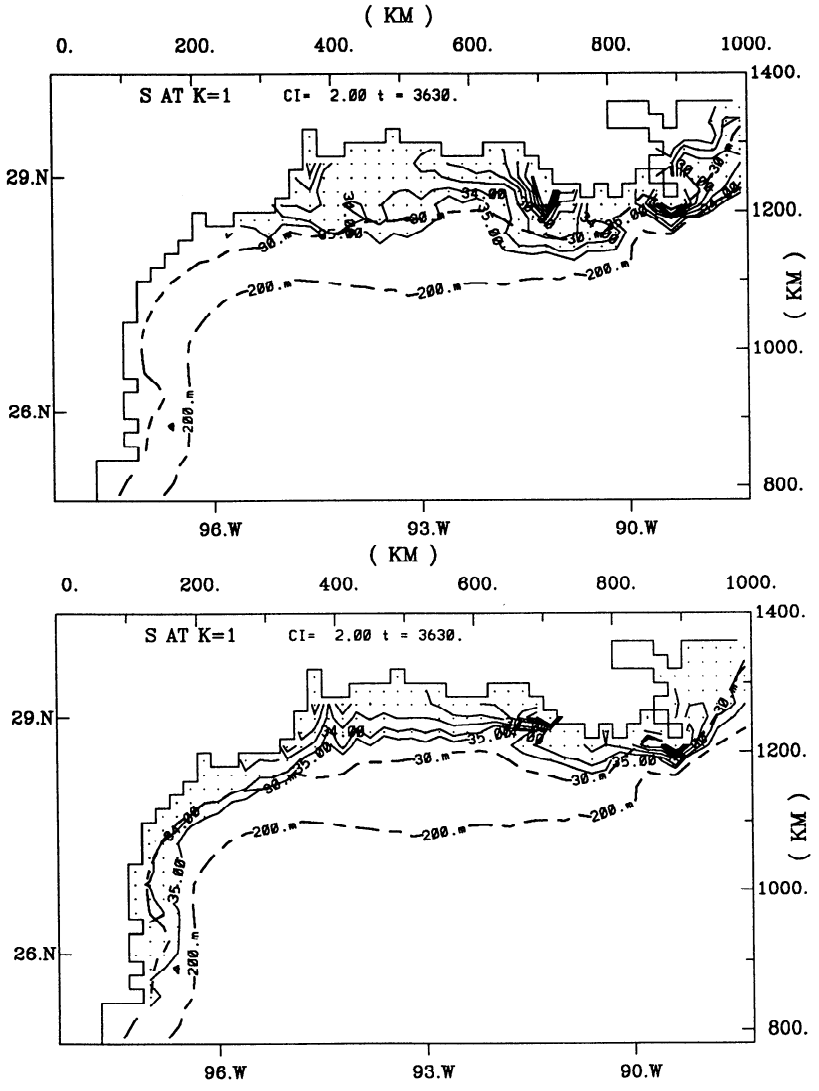

Figure 12. Surface salinity contours (stippled where $S < 35$ practical salinity units) at $t = 3630$ days for solutions (top) without and (bottom) with wind.

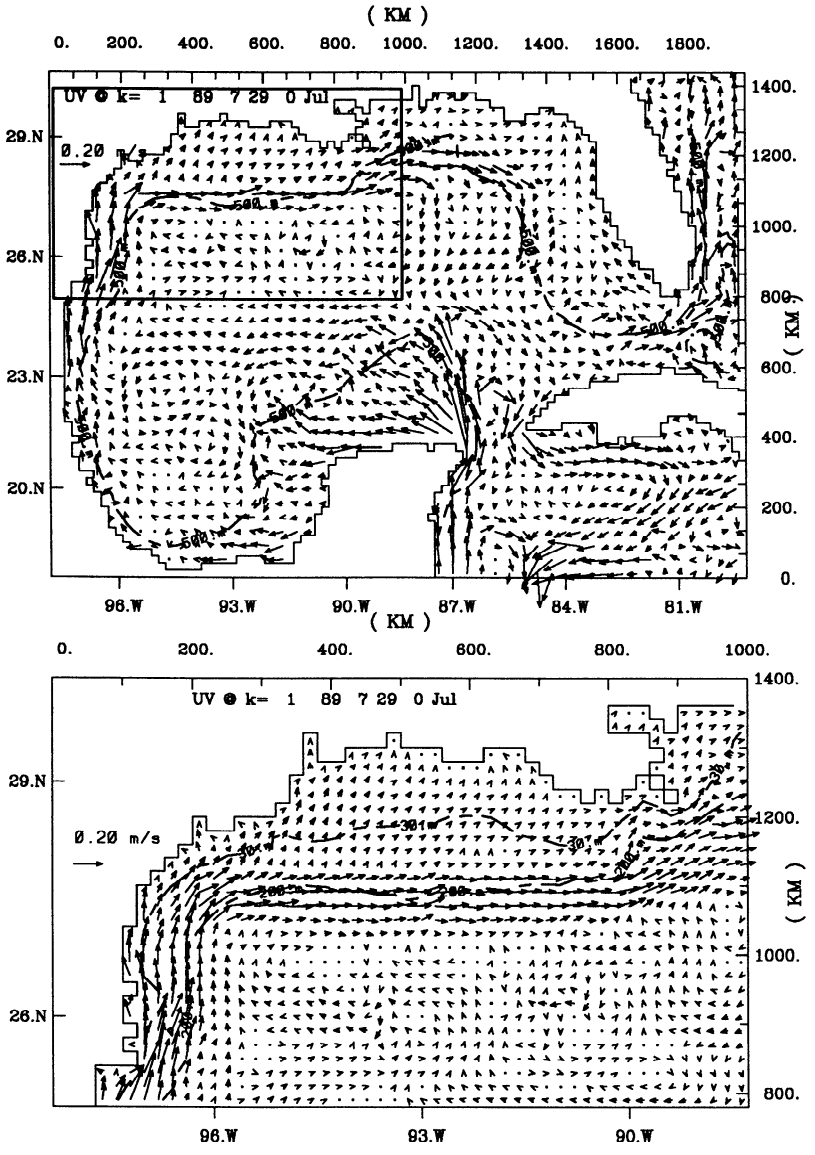

Figure 13. The July-mean near-surface currents for variable wind experiment (case 1) for (top) the entire domain and (bottom) enlarged LATEX region.

over that produced by wind and the additional discharge (~0.02 Sv) alone. In both cases 1 and 2, transport increases westward, consistent with onshore flux over the outer shelf and shelf break.

5.3. Eddy Versus Wind Versus River Buoyancy

Since westward wind and shelf transport are closely related, we can estimate from Figure 16 the shelf transport that would result had the model been forced by the climatological wind stress used for Figure 2 (~0.3 dyn cm^{-2}), with river but no LCEs. The result is shown in Figure 16 as upper and lower bounds in March. At 90.5°W the values bracket those of the LCES case (Figure 16, star symbols). At 95.2°W, LCEs increase the transport values by 0.04 to 0.08 Sv, 35 to 100% over the values produced by wind (and river buoyancy). On the other hand, we have seen in Figure 11 that eddies alone do not contribute to shelf transport. Therefore the increased transport must be due to onshore flux V over the outer shelf and shelf break by the combined effect of LCEs and wind. This may be in the form of $V = -\tau^x \delta_E/\rho_0(f + \zeta)$, where δ_E is the Ekman depth and f is the Coriolis parameter. For westward wind ($\tau^x < 0$) the cross-slope flux increases in the presence of a LCE ($\zeta < 0$) over the slope. Besides directly increasing the shelf transport, this flux results in onshore heat transport and increased stratification, which in turn produce more intense westward current. This inference is supported by the stream function plot of Figure 10a, obtained by subtracting the "eddy plus river" solution from the "eddy plus wind plus river" solution. This gives almost identical transport values (on the shelf) as those obtained from Figure 2. The plot also does not show a wind curl driven shelf break current which, being already weak in winter (Figure 14), is now effectively canceled by the more intense westward flow because of increased stratification. Thus wind/eddy interaction does not cancel when taking the difference. The inference is also consistent with the plot of

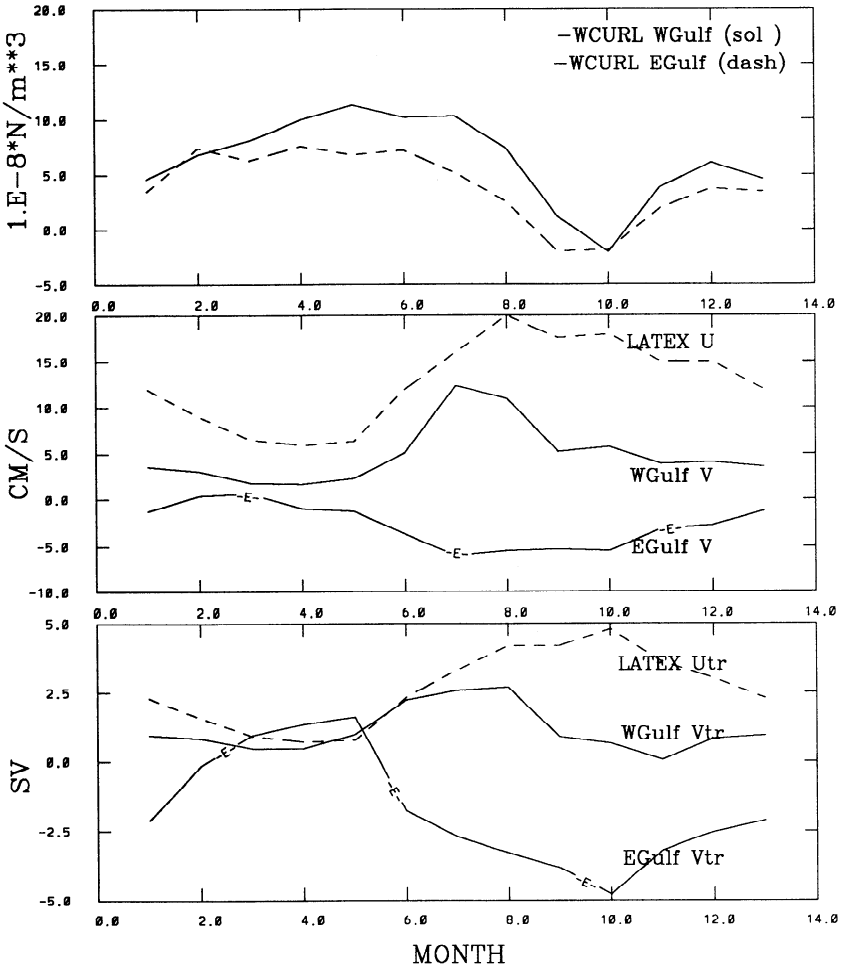

Figure 14. Monthly variations of (top) the wind stress curl averaged over 93°–96°W and 23°–26°N (WGulf) and over 86°–89°W and 26°–28°N (EGulf); (middle) maxima of the currents between 93° and 96°W (averaged from 23° to 26°N, WGulf V), between 86° and 89°W (averaged from 26° to 28°N; EGulf V, negative "maximum"), and between 27° and 28°N (zonally averaged from 91° to 94°W, LATEX U); and (bottom) transports in the direction of the maximum currents and averaged over the three regions.

Oey et al. [1992], which showed a scenario of enhanced onshore flux across the shelf break when westward wind acted on a LCE propagating westward over the LATEX slope.

6. Conclusions

I have used numerical experiments to explain how the observed cyclonic gyre on the LATEX shelf may be set up by LCEs, wind, and river buoyancy. Westward current shoreward of the gyre is primarily due to wind, but all three types of forcing contribute to the amount of transport. At the peak transport in October, for example, the wind, river, and LCE contributions are 0.1 Sv, 0.07 Sv, and 0.04 to 0.08 Sv, respectively (Figure 16). These values vary with season because transport depends on the strength of the westward component of the wind and because contributions from river buoyancy and LCEs depend on their interaction with the wind. Thus westward shelf transport is small during the summer months when wind is primarily from the south. While the contribution from interaction between buoyancy and wind is relatively well understood, that between LCEs and wind is not and deserves a more thorough study.

Flows on the other three sides of the gyre are driven by a combination of wind and eddies. Both LCEs (Figure 11) and summertime wind (Figure 15) cause flow convergence in the southwestern shelf and produce eastward current along the shelf break. LCEs account for shoreward intrusion near the Mississippi Canyon (Figure 11).

The model showed that LC expansion and propagation and decay of LCEs, with timescales of a few months to 1 to 2 years, all contribute to forcing the SC. The SC may therefore be considered as being quasi-steady driven by the totality of effects from the LCEs and seasonally modulated by the wind, so that it is most intense during late summer and fall and weakest in winter. The SC transport due to LCEs is ~4 Sv (Figure 2), which dominates the transport due to wind curl, for all months except fall, when they contribute equally (Figure 14).

Observational evidence of an eastward shelf break current is given by CK, who also cited a number of previous studies. Moreover, they (as well as others) found that along-shelf winds correlate well with along-shelf currents for regions west of ~92.5°W. To the east, *Chuang and Wiseman* [1983] found, on the other hand, that the correlation is poor. The

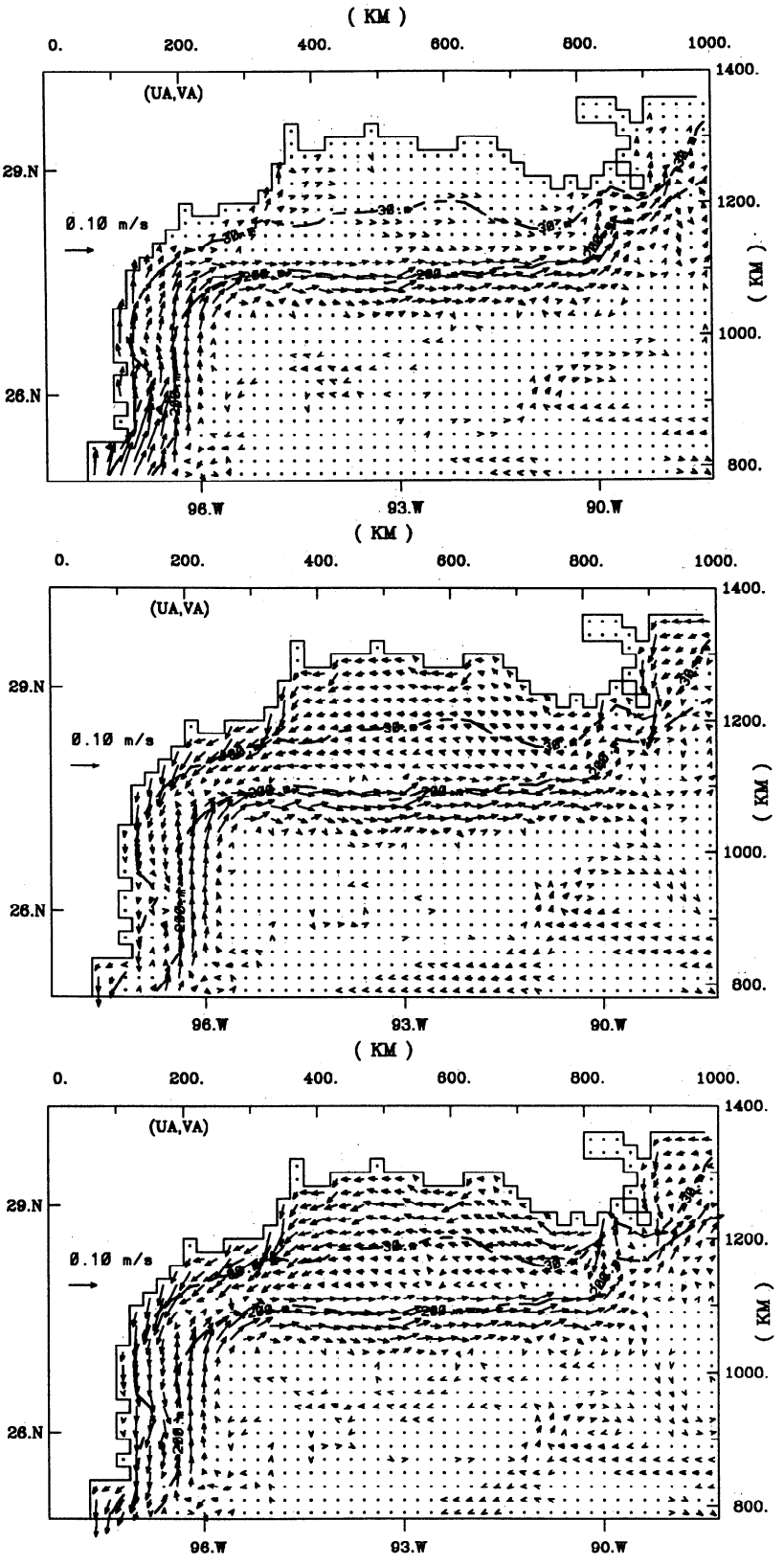

Figure 15. Depth-averaged vectors for (top) July, (middle) October without rivers, and (bottom) October with rivers.

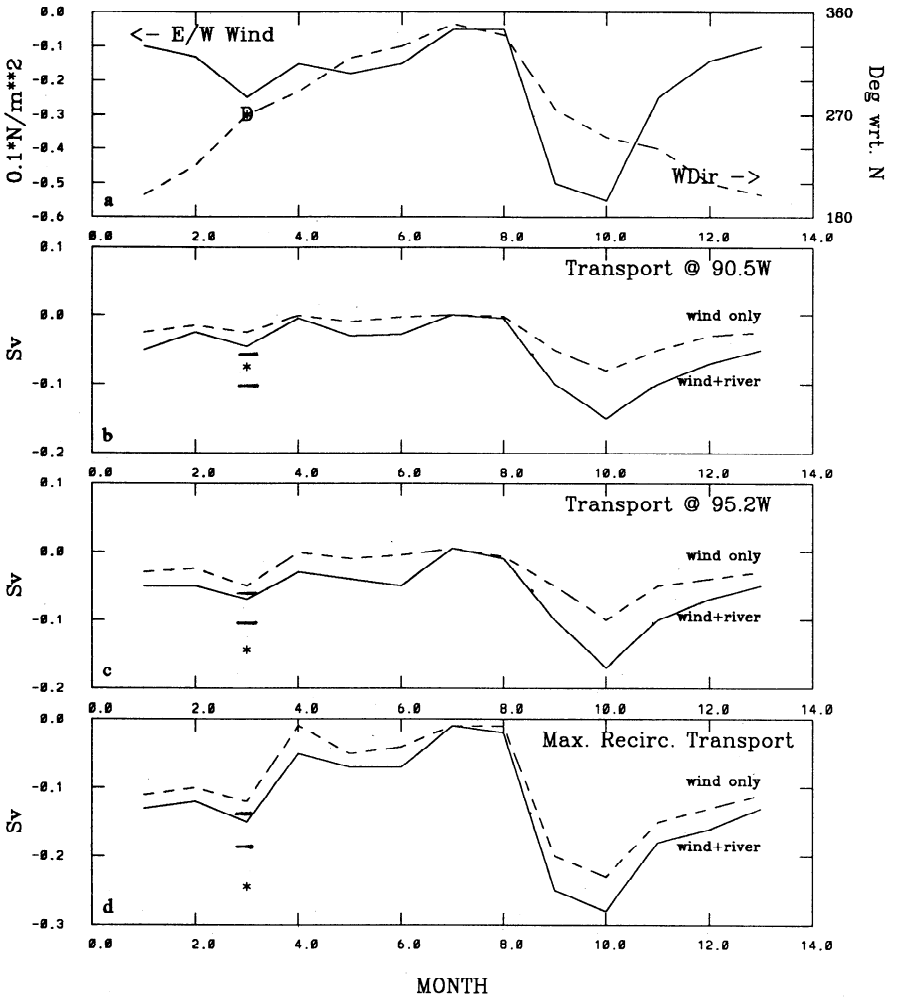

Figure 16. Time series of the (a) east/west wind stress and direction (toward which the wind blows, measured clockwise from true north), (b) westward transports (integrated from shore to the 30-m isobath) at 90.5°W and (c) at 95.2°W for both the wind-only and wind plus river cases, and (d) maximum recirculation transport (centered near 94.5°W, 28°N, compare Figure 2). Stars denote values for the eddy plus wind plus river case (i.e., Figure 2) with D denoting wind direction.

present results suggest that the poor correlation there may be due to the dominance of both along-canyon intrusion and buoyancy processes (Figures 11 and 12).

Finally, the model shows a seasonal boundary current in the western Gulf, driven by the wind stress curl. The WBC is strongest in July–August, 1 to 2 months after the maximum (negative) wind stress curl. This response agrees with *Sturges*' [1993] results. The SC is driven in part by the WBC and in part by the wind stress curl in the eastern Gulf.

Acknowledgments. This work was funded by the Mineral Management Service (COTR, Bob Labelle) via Dynalysis of Princeton. I am grateful to comments from two anonymous reviewers and benefited from comments on the draft manuscript by Chris Mooers, Bob Reid, and Bill Wiseman. Supercomputer time was provided by the Pittsburgh Supercomputing Center and the National Center for Supercomputing Applications, Illinois.

References

Blumberg, A. F., and G. L. Mellor, Diagnostic and prognostic numerical circulation studies of the South Atlantic Bight, *J. Geophys. Res.*, *88*, 4579–4592, 1983.

Brooks, D. A., Current and hydrographic variability in the northwestern Gulf of Mexico, *J. Geophys. Res.*, *89*, 8022–8032, 1984.

Chuang, W., and W. J. Wiseman Jr., Coastal sea level response to frontal passages on the Louisiana-Texas shelf, *J. Geophys. Res.*, *88*, 2615–2620, 1983.

Cochrane, J. D., and F. J. Kelly, Low-frequency circulation on the Texas-Louisiana continental shelf, *J. Geophys. Res.*, *91*, 10,645–10,659, 1986.

Csanady, G. T., The arrested topographic wave, *J. Phys. Oceanogr.*, *8*, 47–62, 1978.

Fargion, G. S., and R. W. Davis, Gulfcet cruise 06 hydrographic data, *Tech. Rep. 94-02-T*, 144 pp., Dep. of Mar. Biol. Texas A&M Univ. Galveston, 1994.

Levitus, S., Climatological atlas of the world ocean, *NOAA Prof. Pap. 13*, 173 pp., U.S. Govt. Print. Office, Washington, D. C., 1982.

Oey, L.-Y., Loop current and eddies: 3-D model experiments and analyses, *Ocean Model. Group Rep. 15*, 42 pp., and 30 figures, Stevens Inst. of Technol., Hoboken, N. J., 1994.

Oey, L.-Y., and P. Chen, A model simulation of circulation in the northeast Atlantic shelves and seas, *J. Geophys. Res.*, *97*, 20,087–20,115, 1992a.

Oey, L.-Y., and P. Chen, A nested-grid model simulation of the Norwegian Coastal Current, *J. Geophys. Res.*, *97*, 20,063–20,086, 1992b.

Oey, L.-Y., Y.-H. Zhang, and H. Lee, The circulation on the

Louisiana-Texas continental shelf: A three-dimensional model study (abstract), *Eos Trans. AGU*, *73*(14), Spring Meeting suppl., 158, 1992.

Shi, C., and D. Nof, The splitting of eddies along boundaries, *J. Mar. Res.*, *51*, 771–795, 1993.

Sturges, W., The annual cycle of the western boundary current in the Gulf of Mexico, *J. Geophys. Res.*, *98*, 18,053–18,068, 1993.

Wright, L. D., and J. M. Coleman, Effluent expansion and interfacial mixing in the presence of a salt wedge, Mississippi River delta, *J. Geophys. Res.*, *76*, 8649–8661, 1971.

L.-Y. Oey, Program in Atmospheric and Oceanic Sciences, Princeton University, Sayre Hall, Forrestal Campus, Princeton University, Princeton, NJ 08544. (e-mail: lyo@kuroshio.princeton.edu)

(Received June 9, 1994; revised January 12, 1995; accepted February 20, 1995.)